JOURNAL OF GUIDANCE, CONTROL, AND DYNAMICS
Vol. 44, No. 12, December 2021

Engineering Notes

Trajectory Design for Proximity Operations: The Relative Orbital Elements' Perspective

Gabriella Gaias* and Marco Lovera†
Politecnico di Milano, 20156 Milan, Italy

https://doi.org/10.2514/1.G006175

I. Introduction

THE need to preserve commercial and scientific relevant orbits in the low Earth belt asks for the active removal of inoperative satellites, which lay on slowly decaying orbits and typically present a moderate eccentricity value [1]. Proximity operations around non-cooperative targets require the capability to execute prompt inbound/receding trajectories as well as a certain level of autonomy to react in an operationally safe fashion. The guidance and control strategies developed for docking cooperative craft can hardly be used in this case for operational reasons. As a result, the study of control solutions applicable to close-range proximity operations and suitable for spaceborne implementation is an active research field.

Relative orbital elements (ROEs) are one of the many existing sets of variables to describe the relative dynamics between satellites orbiting around the same main attractor. With reference to the survey [2], the ROEs used in this work are the quasi-nonsingular ROEs based on relative eccentricity/inclination vectors. For formation-flying and space rendezvous applications where the satellites are separated from few to several tens of kilometers, this is a convenient choice to reduce the linearization errors, to include the effect of orbital perturbations [3], and to exploit the methods of celestial mechanics to identify the most efficient locations of the orbit correction maneuvers [4]. As ROEs are nonlinear functions of the nonsingular orbital elements, they are slowly varying variables. Moreover, they merge the physical insight in the absolute orbits with a straightforward visualization of the relative motion in the local Cartesian orbital comoving frame—the Hill frame. Lastly, recalling their origin from the study of satellite co-location on geostationary orbits, they allow to compute easily the minimum distance between the two satellites over one orbital period in the plane perpendicular to the velocity. As explained in [5], this quantity is related to the difference of phase angles of the relative eccentricity/inclination vectors for almost bounded relative orbits. In the presence of a nonvanishing relative semimajor axis, instead, its expression is derived in [6]. This one-orbit minimum distance plays a crucial role to assess the safety of a formation in the presence of navigation uncertainties in the along-track direction [7]. To date these ROEs have been widely exploited to support the flight dynamics activities and to design the spaceborne guidance navigation and control (GNC) systems of a large number of formation-flying missions flown in low Earth orbits (e.g., GRACE formation switch, TerraSAR-X–TanDEM-X, PRISMA, AVANTI) [8].

In the close-range domain (when the intersatellite separation is less than 1 km), the relative dynamics is often described using the Cartesian relative state composed by position and velocity. For the Keplerian near-circular case, the linearized equations of the relative motion have been first derived in [9] and extensively used since then. These are known as the Hill–Clohessy–Wiltshire (HCW) equations. In the close-range domain, where small relative distances and short time scales limit the impact of errors due to simplifications and non-Keplerian effects, the HCW equations are widely used thanks to the existence of a simple solution (i.e., they are a system of first-order differential equations with constant coefficients). The presence in the state of the Cartesian relative position eases the modeling of the field of view of the sensors and of the path constraints of the approach corridor. Moreover, for the phases of forced motion, the continuous control acceleration profile can be computed using the convolution matrix. Nevertheless, the Cartesian relative position and velocity state is composed of fast varying variables.

This Note aims at merging advantages from both the two mentioned approaches in the specific application of close-range proximity operations. Previous research already identified some points of connection that were then exploited to derive specific results. In [10] it was shown that the linearized relative dynamics described either in the local Cartesian frame or through orbital elements' differences share equivalence through a linearized transformation. This was used to calibrate the initial conditions in Cartesian state to reduce the subsequent propagation error. In [11] it was recognized that ROEs can be written as functions of the integration constants of the HCW equations. This was used to derive an effective and simple interpretation of the geometry of the natural solutions of the HCW equations in terms of the ROE components. Such underlying mapping from ROEs to the Cartesian relative state has been then used in [12] to derive a general empirical formulation to include the mean effects produced by nonconservative perturbations onto the relative motion in ROEs. Despite these results, the definition of a rigorous formal transformation to prove the equivalence of such formulations was lacking. It is here shown that the geometrical mapping of the ROEs in the local Hill frame is *de facto* the change of variables sought. By applying it, the matrices of the plant, input control, state transition, and convolution are consistently transformed back and forth. Because the change of variables is time-varying, it matches the fact that ROEs derive from expanding the orbital elements of the reference absolute orbit (which are defined in an inertial frame), whereas the Cartesian relative state is defined into the local Hill frame (which rotates at the rate of the mean motion). Accordingly, results from linear control theory can be interpreted under the perspective of astrodynamics. Conversely, observations about the optimal locations of the maneuvers based on the Gauss's variational equations can be used to define the distribution over time of the control points. In this context, this Note presents a methodology to generate piecewise constant acceleration profiles from an impulsive guidance solution, setting up a control grid that minimizes the difference between impulsive and equivalent delta-v burns corresponding to the acceleration profile. This allows tackling and solving the simpler problem based on the impulsive approximation, while exploiting results and insight in the solution that are available from impulsive analysis in the ROE framework. The goal is to produce solutions feasible for spaceborne autonomous implementations as well as to aid the definition of safety checks during autonomous operations. As an example the synchronized relative motion with respect to a spinning target satellite is taken and a map of the delta-v required for the 3D fly-around solutions is generated.

Received 3 May 2021; revision received 17 June 2021; accepted for publication 26 June 2021; published online Open Access 21 September 2021.

*Full Professor, Department of Aerospace Science and Technology, Via La Masa 34.

†Research Engineer, Department of Aerospace Science and Technology, Via La Masa 34.

The Note is organized as follows. After a brief recall of definition and properties of the ROEs (Sec. II), Sec. III introduces the unified ROE-HCW framework and revisits under this perspective known results of natural solutions. Section IV addresses the controlled relative motion to deliver a method of synthesis of the piecewise continuous profile of control accelerations, when a reconfiguration guidance profile is designed in either the Cartesian frame or the ROE space.

II. Background

The dimensionless ROEs are defined as [12,13]

$$\begin{aligned}\delta\boldsymbol{\alpha} &= \left(\delta a, \delta\lambda, \delta e_x, \delta e_y, \delta i_x, \delta i_y\right)^T \\ &= \left(\Delta a/a_c, \Delta u + \Delta\Omega\cos i_c, \Delta e_x, \Delta e_y, \Delta i, \Delta\Omega\sin i_c\right)^T \end{aligned} \quad (1)$$

where $\boldsymbol{\alpha} = (a, u, e_x, e_y, i, \Omega)^T$ is the set of Keplerian nonsingular elements, $e_x = e\cos\omega$ and $e_y = e\sin\omega$ are the x and y components of the eccentricity vector, $u = \omega + M$ is the spacecraft mean argument of latitude, a is the semimajor axis, ω is the argument of the perigee, M is the mean anomaly, and i is the inclination. In Eq. (1), the symbol Δ denotes the difference between quantities of the two satellites, respectively, named the chief (c) and the deputy. The term $\delta\lambda$ is called the relative mean argument of longitude, whereas $\delta\boldsymbol{e}$ and $\delta\boldsymbol{i}$ are the relative eccentricity and relative inclination vectors, respectively. By introducing a polar notation for both $\delta\boldsymbol{e}$ and $\delta\boldsymbol{i}$, the phase angles defined from the axes through the ascending node of the chief satellite have, respectively, the meaning of perigee φ and ascending node θ of the relative orbit [7,13].

In particular, as explained in [5], the relative inclination vector $\delta\boldsymbol{i}$ is directed as the unit non-coplanar vector between the orbits of the chief and the deputy. When the differences in inclination and right ascension of the ascending node are small, its components are given as in Eq. (1). The phase angle θ corresponds to the true argument of latitude of the intersection point of the plane-change maneuver between the chief and deputy orbits. The magnitude of the relative inclination vector, instead, is given by the angle between the two orbital planes computed with the spherical trigonometry at the intersection point. The relative eccentricity vector defined in Eq. (1) is the difference of the x and y components of the eccentricity vectors of the chief and deputy satellites, having assumed that their orbital planes almost coincide (i.e., Δi and $\Delta\Omega \ll 1$).

The Keplerian relative dynamics in ROEs is modeled by the following system:

$$\begin{cases}\delta\dot{\boldsymbol{\alpha}} = \mathrm{A}\delta\boldsymbol{\alpha} + \mathrm{B}\tilde{\boldsymbol{u}} \\ \delta\boldsymbol{\alpha}(t_0) = \delta\boldsymbol{\alpha}_0\end{cases}, \qquad \mathrm{A} = \begin{bmatrix} 0 & 0 & 0 & 0 & 0 & 0 \\ -\frac{3}{2}n & 0 & 0 & 0 & 0 & 0 \\ 0 & 0 & 0 & 0 & 0 & 0 \\ 0 & 0 & 0 & 0 & 0 & 0 \\ 0 & 0 & 0 & 0 & 0 & 0 \\ 0 & 0 & 0 & 0 & 0 & 0 \end{bmatrix},$$

$$\mathrm{B} = \frac{1}{na}\begin{bmatrix} 0 & 2 & 0 \\ -2 & 0 & 0 \\ +\sin u & 2\cos u & 0 \\ -\cos u & 2\sin u & 0 \\ 0 & 0 & \cos(u) \\ 0 & 0 & \sin(u) \end{bmatrix} \quad (2)$$

where $\tilde{\boldsymbol{u}}$ is the vector of the control accelerations written in the radial–tangential–normal (RTN) frame, with R positive outward with respect to the center of the Earth and N directed as the orbital angular momentum. For near-circular orbits the transverse direction almost coincides with the one of the velocity (here referred to as tangential direction). Moreover, n is the mean motion of the chief craft.

For the sake of completeness, also the linear time-invariant formulation of the HCW equations is as follows:

$$\begin{cases}\dot{\boldsymbol{x}} = \hat{\mathrm{A}}\boldsymbol{x} + \hat{\mathrm{B}}\,\tilde{\boldsymbol{u}} \\ \boldsymbol{x}(t_0) = \boldsymbol{x}_0\end{cases}, \qquad \hat{\mathrm{A}} = \begin{bmatrix} 0 & 0 & 0 & 1 & 0 & 0 \\ 0 & 0 & 0 & 0 & 1 & 0 \\ 0 & 0 & 0 & 0 & 0 & 1 \\ 3n^2 & 0 & 0 & 0 & 2n & 0 \\ 0 & 0 & 0 & -2n & 0 & 0 \\ 0 & 0 & -n^2 & 0 & 0 & 0 \end{bmatrix},$$

$$\hat{\mathrm{B}} = \begin{bmatrix} 0 & 0 & 0 \\ 0 & 0 & 0 \\ 0 & 0 & 0 \\ 1 & 0 & 0 \\ 0 & 1 & 0 \\ 0 & 0 & 1 \end{bmatrix} \quad (3)$$

III. Unified ROE-HCW Framework for the Keplerian Motion

Inspired by the fact that ROEs can be written as functions of the integration constants of the HCW equations [11] and from the linearized-relative-orbit-element variational equations developed in [14], to study how such invariants of the HCW equations vary over time when subject to external accelerations, the unified ROE-HCW framework for the close-range domain is obtained as follows. The change of variables (Lyapunov transformation) $\mathrm{T}(t)$ is introduced:

$$\mathrm{T}(t) = \begin{bmatrix} 1 & 0 & -\cos(nt) & -\sin(nt) & 0 & 0 \\ 0 & 1 & 2\sin(nt) & -2\cos(nt) & 0 & 0 \\ 0 & 0 & 0 & 0 & \sin(nt) & -\cos(nt) \\ 0 & 0 & n\sin(nt) & -n\cos(nt) & 0 & 0 \\ -(3n)/2 & 0 & 2n\cos(nt) & 2n\sin(nt) & 0 & 0 \\ 0 & 0 & 0 & 0 & n\cos(nt) & n\sin(nt) \end{bmatrix} \quad (4)$$

where the rows of $\mathrm{T}(t)$ transform the ROE set defined in Eq. (1), respectively, in the RTN components of the relative position and relative velocity. The transformation $\mathrm{T}(t)$ is nonsingular for all t as the determinant is constant and equal to $n^3/2$. Note also that both $\mathrm{T}(t)$ and $\mathrm{T}^{-1}(t)$ are continuously differentiable. Accordingly, the inverse transformation is given by

$$\mathrm{T}^{-1}(t) = \begin{bmatrix} 4 & 0 & 0 & 0 & 2/n & 0 \\ 0 & 1 & 0 & -2/n & 0 & 0 \\ 3\cos(nt) & 0 & 0 & \frac{\sin(nt)}{n} & 2\frac{\cos(nt)}{n} & 0 \\ 3\sin(nt) & 0 & 0 & -\frac{\cos(nt)}{n} & 2\frac{\sin(nt)}{n} & 0 \\ 0 & 0 & \sin(nt) & 0 & 0 & \frac{\cos(nt)}{n} \\ 0 & 0 & -\cos(nt) & 0 & 0 & \frac{\sin(nt)}{n} \end{bmatrix} \quad (5)$$

so that

$$\boldsymbol{x} = \mathrm{T}(t)a\delta\boldsymbol{\alpha} \qquad a\delta\boldsymbol{\alpha} = \mathrm{T}^{-1}(t)\boldsymbol{x} \quad (6)$$

where the semimajor axis of the chief scales $\delta\boldsymbol{\alpha}$ to set all the quantities in the unit of the length. By using this change of variables, it holds

$$\Phi(t,t_0)=\mathrm{T}^{-1}(t)\hat{\Phi}(t,t_0)\mathrm{T}(t_0) \qquad \hat{\Phi}(t,t_0)=\mathrm{T}(t)\Phi(t,t_0)\mathrm{T}^{-1}(t_0)$$
$$\mathrm{A}=\mathrm{T}^{-1}(t)\hat{\mathrm{A}}T(t)-\mathrm{T}^{-1}(t)\dot{\mathrm{T}}(t) \qquad \hat{\mathrm{A}}=\mathrm{T}(t)\mathrm{A}\mathrm{T}^{-1}(t)-\mathrm{T}(t)\dot{\mathrm{T}}^{-1}(t)$$
$$a\mathrm{B}=\mathrm{T}^{-1}(t)\hat{\mathrm{B}} \qquad \hat{\mathrm{B}}=\mathrm{T}(t)a\mathrm{B}$$
$$\Psi=\mathrm{T}^{-1}(t)\hat{\Psi} \qquad \hat{\Psi}=\mathrm{T}(t)\Psi \tag{7}$$

where $\hat{\cdot}$ quantities refer to the HCW dynamics, whereas the others to their respective in ROEs. Φ is the state transition matrix, whereas Ψ is the convolution matrix. The term

$$\mathrm{T}^{-1}(t)\dot{\mathrm{T}}(t)=\begin{bmatrix}0&0&0&0&0&0\\0&0&0&0&0&0\\0&0&0&n&0&0\\0&0&-n&0&0&0\\0&0&0&0&0&n\\0&0&0&0&-n&0\end{bmatrix} \tag{8}$$

represents a rotation of the relative eccentricity and inclination vectors at the rate of the mean motion and matches the fact that the ROEs are defined in the inertial frame, whereas the Cartesian relative state is defined into the local orbital comoving frame. Note that due to the presence of this term the change of variable T differs from the one proposed in [15] to transform the in-plane HCW equations into two uncoupled, second-order, linear differential equations in the new variables.

Several useful relative orbits for formation flying are derived from the solution of Eq. (2) or Eq. (3). To show the whole information that is conveyed by the unified framework, two cases are here shown. The first example (depicted in Fig. 1) is a passively safe relative orbit, typically used for approaching non-cooperative targets (e.g., AVANTI) or for interferometry (e.g., TanDEM-X–TerraSAR-X). The second example (depicted in Fig. 2) is a projected circular orbit: a bounded, centered, relative orbit whose projection on the T-N plane is a circle.

The plots in the (a)-view of Figs. 1 and 2 show the 3D trajectory (in black) in the RTN frame. Note that the axes are oriented in agreement with the physical sense of a satellite flying along its orbit: the radial is the vertical axis (local vertical direction), with the Earth at the bottom of the page. The thicker part of the 3D orbit is the portion above the chief's orbital plane (i.e., with positive normal component). To aid the visualization of the trajectory, the orbital plane (R-T) is highlighted and the in-plane projection is plotted in gray. The remaining projections are shown in green for the T-N plane and in blue for the R-N plane. The blue line provides an immediate understanding of the safety of the formation that is whether the deputy satellite will cross

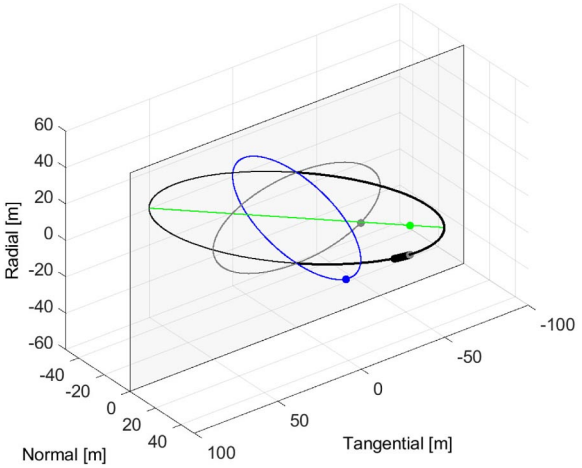

a) RTN view.

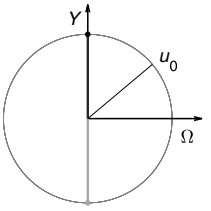

δe (black), $\phi = 90°$

δi (gray), $\theta = -90°$

$u_0 = 40°$

b) XY view.

Fig. 1 Passive safe orbit $a\delta\alpha$ = (0, 0, 0, 25, 0, −50) m.

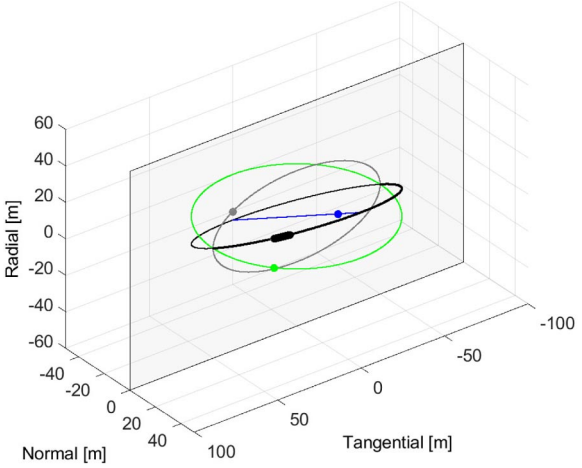

a) RTN view.

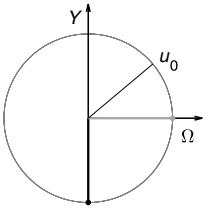

δe (black), $\phi = -90°$

δi (gray), $\theta = 0°$

$u_0 = 40°$

b) XY view.

Fig. 2 Projected circular orbit $a\delta\alpha$ = (0, 0, 0, −25, 50, 0) m.

the origin during one revolution. Larger dots on the projections identify the position at initial time; on the 3D trajectory they also allow understanding the direction of traveling of the deputy satellite. In the case of Fig. 1, the orbit is bounded (i.e., $\delta a = 0$) and centered with respect to the chief (i.e., $\delta\lambda = 0$). Passive safety is achieved by phasing the relative eccentricity inclination vectors in an (anti)parallel fashion [5,7]: $\theta = \varphi \pm z\pi$, with $z \in \mathbb{N}$. Among all the possible combinations, a convenient choice is to set $\delta i_x = 0$, to cancel the mean effect due to J_2 on the relative inclination vector. The chosen case is of this kind (see $a\delta\boldsymbol{\alpha}$ in the caption). The second example of Fig. 2 is typically used in interferometry when a baseline of constant length is needed in the plane perpendicular to the radial direction. Once imposed this constraint, the ROE state has the structure of $a\delta\boldsymbol{\alpha} = (0, 0, 0, -k/2, k, 0)$. Accordingly, there are no degrees of freedom left, and thus it is not possible to mitigate the effect of the mean perturbation due to J_2.

The visualization of the geometry of the relative trajectory is more straightforward using the Cartesian state formulation. The ROEs, in fact, convey only the size (δe) and position ($\delta a, \delta\lambda$) of the center of the in-plane ellipse, the maximum amplitude of the out-of-plane motion (δi), and the amount of the minimum distance to the origin on the R-N plane ($\delta\boldsymbol{e}^T\delta\boldsymbol{i}$) [7,11,13]. On the other hand, the ROEs provide additional information related to the absolute orbit of the chief. The (b)-view of Figs. 1 and 2 shows the relative eccentricity (in black) and inclination (in gray) unit-vectors in the orbital planes of the satellites ($\Omega_c \cong \Omega_d$, $i_c \cong i_d$). From this plot, one can obtain the following additional information: the $\delta\boldsymbol{e}/\delta\boldsymbol{i}$ phasing (related to formation safety) and the moment along the orbit (u) when the maximum separations in R (i.e., $u = \varphi + z\pi$), T (i.e., $u = \varphi + \pi/2 + z\pi$), and N (i.e., $u = \theta + z\pi$) are reached. Moreover, because it is known how $\delta\boldsymbol{e}$ and $\delta\boldsymbol{i}$ move due to the mean effect of orbital perturbations (e.g., Earth oblateness) one can predict how the motion will be affected over time [11–13]. Note that the Ω-Y plane is often denoted as $\delta\cdot_x$-$\delta\cdot_y$ plane when designing guidance and control schemes directly in the ROE space [4,13,16]. Therefore, known current and aimed directions of the relative eccentricity and inclination vectors, the mean argument of latitude u at which performing the maneuver is simply the phase angle (measured from the Ω axis) of the ROE difference vector. This provides the additional flight dynamics information about possible time and corresponding location on the chief's orbit of the required maneuvers.

The change of variable T is strictly valid for the Keplerian motion and performs the back-and-forth transformation of the relative Cartesian state into the osculating ROEs. The modeling of the geopotential effects (the major perturbation in low terrestrial orbits) is detailed in [3], whereas the mapping of ROEs into the Cartesian frame (also applicable at large intersatellite separations) is discussed in [17]. Nevertheless, when the intersatellite distance is definitely below 1 km, a quick assessment of the effect produced by J_2 can be obtained by mapping directly the mean ROEs through T, because the closer the satellites the more effective is the natural cancellation of the oscillating terms. Accordingly, for projected circular orbits, which represent a worse-case scenario, it amounts to circa 3% of the radius of the circumference in the T-N plane when accumulated over five orbital periods.

IV. Inclusion of Control Accelerations

The reconfiguration and maintenance of a satellite formation is generally achieved by means of impulsive control techniques. This is motivated by the following facts: orbit corrections are mostly of the order of few cm/s, often chemical propulsion systems are employed, and payloads usually ask for extended arcs without maneuvers to avoid interference with the instruments. Impulsive control techniques are often based on the Gauss's variational equations (GVEs), to relate delta-v burns in the RTN frame to instantaneous changes in the orbital elements. In the ROE framework, the control input matrix of Eq. (2) is derived from the GVEs written for the nonsingular orbital elements' set and for circular orbits [11]. This served as basis for the development of delta-v optimal closed-form schemes for formation keeping [13] and reconfiguration [16]. At the practical level, when the prescribed impulsive maneuvers are realized through burns of up to few minutes of duration, the error introduced is still acceptable. This is true also for reconfigurations completed over several orbits, provided that the cumulative effect of J_2 is taken into account by the guidance solution, as, for example, done in [4]. Nevertheless, the refinement of impulsive control techniques to include the finite-time modeling of the burn has been studied in [18] (by performing the analytical integration of the GVE over the burn time) and in [19] (by employing the ROE-based convolution matrix).

The change of ROEs achieved at time t_F after an impulsive delta-v occurred at t_0 is

$$a\Delta\delta\boldsymbol{\alpha} = \Phi(t_F, t_0)a\mathrm{B}\delta\boldsymbol{v} \tag{9}$$

where $\delta\boldsymbol{v}$ is the delta-v vector in RTN. Note that for the Keplerian motion the plant matrix of the dynamics in ROEs is nil-potent of order 2, and therefore $\Phi(t_F, t_0)$ is trivially $(\mathrm{I} + \mathrm{A}(t_F - t_0))$. At a practical level, the propulsion system imparts an acceleration to yield the following equivalent delta-v:

$$\delta v_i = C_i\Delta t = C_i\frac{\Delta u}{n} = C_i\frac{2h_{ba}}{n} \tag{10}$$

where, for each component i, C is a constant acceleration, and Δt is the total burn time corresponding to a change of mean argument of latitude Δu with $2h_{ba}$ the double of half-burn-arc angle. Using Eq. (10) the ROE change is expressed as

$$a\Delta\delta\boldsymbol{\alpha} = \frac{2h_{ba}}{n^2}\begin{bmatrix} 0 & 2 & 0 \\ -2 & -3(u_F - u_0) & 0 \\ \sin u_0 & 2\cos u_0 & 0 \\ -\cos u_0 & 2\sin u_0 & 0 \\ 0 & 0 & \cos u_0 \\ 0 & 0 & \sin u_0 \end{bmatrix}\begin{pmatrix} C_R \\ C_T \\ C_N \end{pmatrix} \tag{11}$$

The convolution matrix in ROEs for a burn starting at u_0 and ending at u_F, with $\Delta u = u_F - u_0$ is

$$\Psi(u_F, u_0) = \frac{1}{n^2}\begin{bmatrix} 0 & 2\Delta u & 0 \\ -2\Delta u & -\frac{3}{2}(\Delta u)^2 & 0 \\ -(c_{u_F} - c_{u_0}) & +2(s_{u_F} - s_{u_0}) & 0 \\ -(s_{u_F} - s_{u_0}) & -2(c_{u_F} - c_{u_0}) & 0 \\ 0 & 0 & +(s_{u_F} - s_{u_0}) \\ 0 & 0 & -(c_{u_F} - c_{u_0}) \end{bmatrix} \tag{12}$$

where a short-hand notation has been used for sine and cosine terms. By taking the mean argument of latitude of the center-of-burn u_c so that $u_c = u_0 + h_{ba}$, the ROE change becomes:

$$a\Delta\delta\boldsymbol{\alpha}(u_F) = \Psi(u_F, u_0)\boldsymbol{C} = \frac{1}{n^2}\begin{bmatrix} 0 & 4h_{ba} & 0 \\ -4h_{ba} & -\frac{3}{2}(2h_{ba})^2 & 0 \\ +s_{u_c}2s_{h_{ba}} & 2c_{u_c}2c_{h_{ba}} & 0 \\ -c_{u_c}2c_{h_{ba}} & 2c_{u_c}2c_{h_{ba}} & 0 \\ 0 & 0 & c_{u_c}2c_{h_{ba}} \\ 0 & 0 & s_{u_c}2s_{h_{ba}} \end{bmatrix}\begin{pmatrix} C_R \\ C_T \\ C_N \end{pmatrix} \tag{13}$$

Thus, modeling a maneuver as impulsive (at u_0) does not affect the δa and $\delta\lambda$ components, but introduces errors on the relative eccentricity and inclination vectors. The latter would be partly reduced by locating the impulsive maneuver at u_c, thus leaving the errors due to the sine/cosine of the half-burn-arc angle. However, the propagation time $t_F - t_c$ (different from $t_F - t_0$) generates then an error on $\delta\lambda$. Note

that the expression of Eq. (13) is equivalent to the one used in Eq. (24) of [18] to refine the control scheme of [13], since the B matrix itself derives from the GVEs. Moreover, the unified ROE-HCW framework established by the change of variables T shows that Ψ is also the transformed of its equivalent in Cartesian variables [see Eq. (7)].

During close-range proximity operations there is the need to perform translational motion in any direction (as, e.g., for the final approach before docking) or fly-around trajectories with respect to any given axis of rotation (as for inspection purposes [20] or for the synchronized motion for active debris removal). These actions require definitely larger maneuvers than formation keeping and reconfiguration, especially when they are performed over limited time windows. Guidance and control algorithms for such phases are typically developed working with the Cartesian state. Accordingly, impulsive guidance solutions are built from the solution of the HCW $\hat{\Phi}$. For inbound/recede straight-line trajectories, the N-maneuvers profile is computed by solving a two-boundary problem for each successive interval $[t_{N_i}, t_{N_{(i+1)}}]$, with two maneuvers occurring at the initial and final times of each interval. For each problem, the complete set of boundary conditions is derived by setting aimed position way points and a desired velocity profile. Examples are the glideslope profile [20] or the one used for the unmanned Automated Transfer Vehicle [21]. These velocity profiles are generated to fulfill technology or safety requirements. Disregarding how the boundary conditions are designed, the computation of the necessary impulsive changes of velocity is performed splitting $\hat{\Phi}$ in its position and velocity subblocks, as explained in [20].

By exploiting the equivalence between HCW equations and ROE-based equations, the computation of the impulsive delta-v burns to realize a given guidance profile defined in the Cartesian frame can be performed directly in the ROE variables, in a more compact fashion. It is formalized as

$$\mathrm{M}\begin{pmatrix}\delta\boldsymbol{v}^i\\ \delta\boldsymbol{v}^{i+1}\end{pmatrix} = na\Big(\delta\boldsymbol{\alpha}(u_{i+1}) - \Phi(u_{i+1},u_i)\delta\boldsymbol{\alpha}(u_i)\Big)$$

$$\mathrm{M} = \begin{bmatrix} 0 & 2 & 0 & 0 & 2 & 0\\ -2 & -3\xi & 0 & -2 & 0 & 0\\ +s_{u_i} & 2c_{u_i} & 0 & +s_{u_i+\xi} & 2c_{u_i+\xi} & 0\\ -c_{u_i} & 2s_{u_i} & 0 & -c_{u_i+\xi} & 2s_{u_i+\xi} & 0\\ 0 & 0 & c_{u_i} & 0 & 0 & c_{u_i+\xi}\\ 0 & 0 & s_{u_i} & 0 & 0 & s_{u_i+\xi}\end{bmatrix} \tag{14}$$

with $\xi = u_{i+1} - u_i$. Note also that $\det \mathrm{M} \neq 0$ if and only if $\xi \neq 0$; i.e., the solution always exists provided that the maneuvers are carried out at distinct time instants. The existence and mitigation of singularities for the 2-burn impulsive solution when in-plane and out-of-plane reconfigurations are treated separately and are discussed in [22].

As an example, consider the straight-line approach along the T direction, referred as V-bar approach, discussed in [20]. This approach requires the deputy to move from −500 to −100 m in approximately 8 minutes. Unlike [20], where the glideslope velocity profile is used to reach the endpoint, here the distance is set to be covered with constant velocity in the available time (resulting in equally spaced position way points on the V-bar). By setting $N = 8$ maneuvers, the solution in the ROE space is shown in Fig. 3a, following the plotting conventions of [16]. The initial ROE state is marked by the black-white bullet; the end one by the red triangle. For the sake of readability, these are also annotated in Fig. 3a. Pre- and postmaneuver ROEs are marked differently to show the effect of each single pulse. The left subplot displays the evolution of the in-plane mean motion (i.e., δa and $\delta\lambda$). Here, the natural relative dynamics make $\delta\lambda$ to drift over time (horizontally), as soon as the relative semimajor axis is not null. The right subplot displays the evolution of the relative eccentricity vector. Note that this view is the Ω-Y

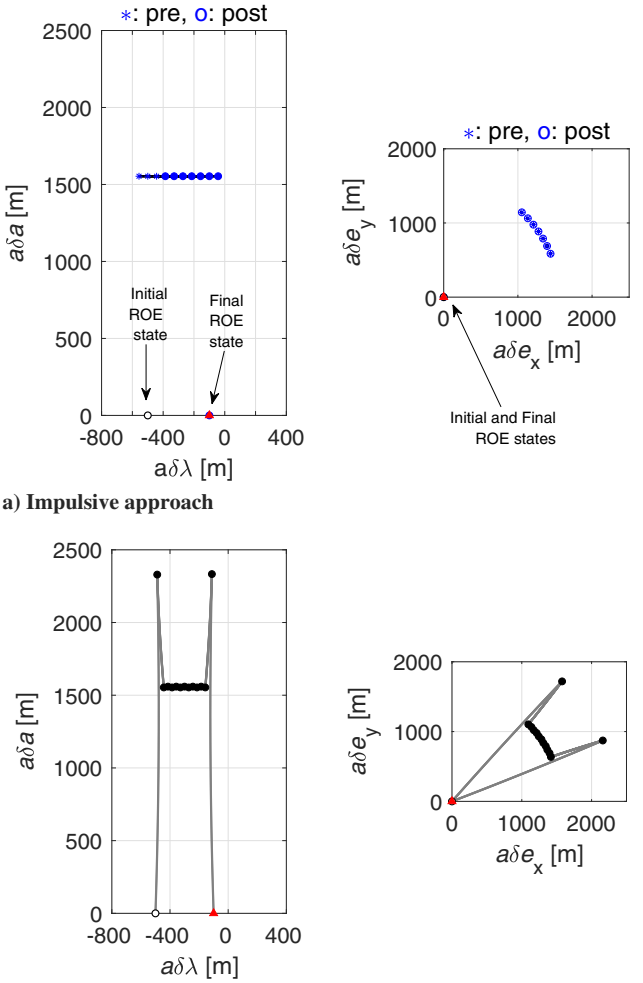

Fig. 3 V-bar: in-plane views of the ROE space.

plane. In the unperturbed case, the relative eccentricity vector is moved only through maneuvers.

The fact that forced motion phases, like the one of the example, require large maneuvers is clear already from the values assumed by the ROEs in Fig. 3. Accordingly, a finite-burn modeling is essential to represent more faithfully the physical realization of the maneuver by means of the propulsion system typically embarked on small-medium satellites. Moreover, given the tight time window, a continuous acceleration profile should be considered.

The same guidance just employed can be used to generate a piecewise constant acceleration profile. Again, for simplicity, the solution is obtained in the equivalent ROE space. The continuous version of the two-point boundary problem of Eq. (14) becomes

$$\Big[\Phi(u_{i+1},u_{\mathrm{int}})\Psi(u_{\mathrm{int}},u_i) \quad \Psi(u_{i+1},u_{\mathrm{int}})\Big]\begin{pmatrix}\boldsymbol{C}^i\\ \boldsymbol{C}^{i+1}\end{pmatrix} = na\Big(\delta\tilde{\boldsymbol{\alpha}}^+_{i+1} - \Phi(u_{i+1},u_i)\delta\tilde{\boldsymbol{\alpha}}^-_i\Big) \tag{15}$$

where $u_{\mathrm{int}} = (u_i + u_{i+1})/2$. The initial/final ROE states are denoted by $\tilde{\cdot}$ to indicate that they are not the same as of Eq. (14) when $i = 2 \ldots N-1$, due to the continuity condition imposed on the state. The in-plane ROEs evolution is displayed in Fig. 3b. Here the intermediate ROE states at u_i (marked in black) are reached continuously as a consequence of the control accelerations.

The trajectories obtained in the two cases are plotted in Fig. 4a: in solid black the impulsive solution, and in dashed gray the continuous one. For the same example, the trajectory obtained implementing the glideslope guidance profile of [20] is shown in Fig. 4b. Irrespective of

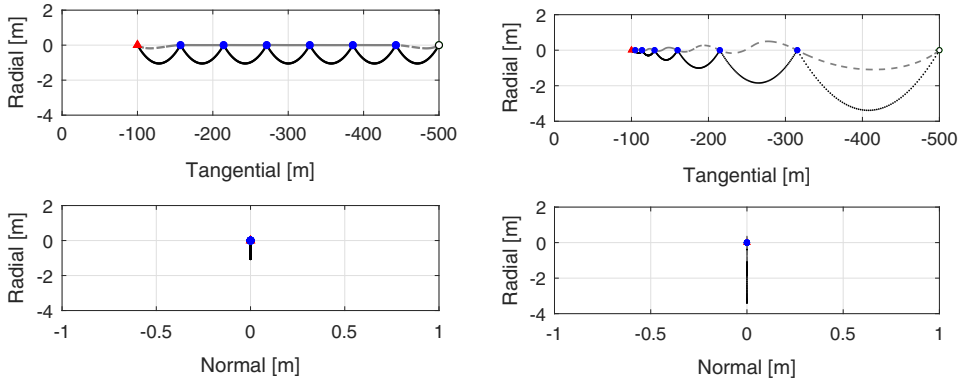

a) Equally spaced way points. b) Glideslope velocity profile.

Fig. 4 V-bar approach: trajectories obtained with impulsive (solid black) and continuous (dashed gray) control.

the strategy used to design the approach, once available the sequence of $\delta\boldsymbol{\alpha}$ (or $\boldsymbol{x}$) at corresponding times, the piecewise constant acceleration profile is computed through Eq. (15) on the $N-1$ intervals.

A. Design of the Control Grid

The accelerations for the two considered examples are displayed in Fig. 5, respectively, in dashed gray and solid black for equally spaced way points and glideslope relative velocity profile. These are obtained solving $N-1$ problems of Eq. (15), which is implementing the control grid sketched in the top part of Fig. 6. There, each full-node corresponds to the location of an impulsive delta-v from the guidance plan (i.e., occurring at u_i). Accordingly, the duration of the shortest piece of constant burn is set by the distance between two consecutive nodes; a quantity linked to the functioning of the propulsion system. Recall that the focus is on reconfigurations that occur over limited time horizons (i.e., fractions of the orbital period) which justifies the use of equally spaced nodes. In Fig. 6, square brackets delimit the ith two-boundaries interval and the dashed vertical line marks the position of u_{int}. Additionally, the centers of burn of the two constant acceleration legs are highlighted (i.e., $u_{c,i}$ and $u_{c,i+1}$). By recalling the insight provided by Eq. (13) on the location of the center-of-burn of a maneuver, it is evident that the *impulsive equivalent* maneuver generated by the continuous acceleration profile is placed in the farthest location, within the limits of the considered interval, from the impulsive maneuvers of the original guidance profile. Accordingly, if the latter was generated to fulfill a delta-v optimal score, its actual continuous realization degrades the original solution due to such discrepancy between the original design and the location of the equivalent impulsive maneuver. As a consequence, the fuel consumption assessed through the original impulsive analysis will not represent the fuel consumption required by its continuous implementation. In light of these considerations, a second grid scheme is provided in the bottom part of Fig. 6. There, the idea is to minimize the difference between the impulsive and piecewise continuous solutions. The rationale is that often the impulsive guidance profile is designed aiming at the minimization of the delta-v consumption. Moreover, it is generally easier to solve the open-loop guidance problem exploiting an impulsive approach rather than tackling directly the continuous problem. The grid control points are still equally spaced, though the intervals are defined to overlap the impulsive burns to the equivalent center-of-burn locations. The approach is straightforward for reconfiguration horizons that do not require to fire at initial and final times (i.e., marked by the empty nodes). Furthermore, it requires some adaptations for the cases in which a trajectory correction is indeed required at the boundary times.

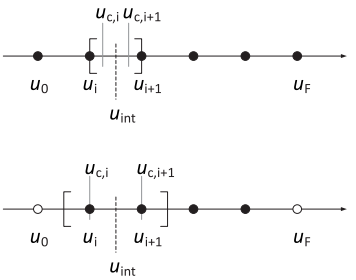

Fig. 6 Possible structures of the control grids: boundary (top) and centered (bottom).

The effect of the choice of the type of control grid when implementing a continuous acceleration to follow an impulsive maneuver plan is considered in the following example. Here, initial and final states in meters are $\delta\boldsymbol{\alpha}_0 = [0, -500, 600, 300, 0, 0]$ and $\delta\boldsymbol{\alpha}_F = [0, -100, 0, 0, 0, 0]$, and semimajor axis of $\approx$7153 km. The reconfiguration is covered in half-orbit-period time and the N grid nodes are equally distributed over the reconfiguration horizon without comprising the initial and final times. The impulsive guidance profile is obtained solving a linear programming problem (in the ROE space) where the 1-norm of the delta-v is minimized. Accordingly, at some nodes no maneuver may occur.

Figure 7 shows the results in terms of trajectory and acceleration profiles, when either boundary grid (solid black) or the centered grid (dashed gray) are used to realize the same impulsive guidance profile. By increasing the number of nodes, the trajectories tend to overlap. Nonetheless, as summarized in Table 1, the equivalent delta-v cost obtained by adopting the centered control grid is cheaper and closer to the budget of the original impulsive guidance profile.

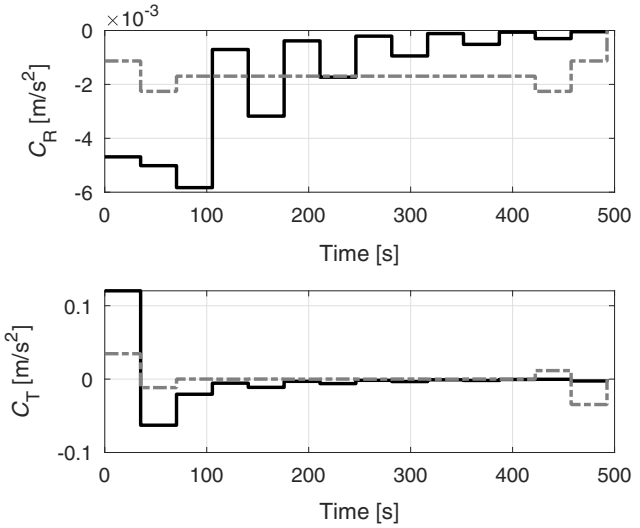

Fig. 5 Acceleration profiles: equally spaced way points (dashed gray) and glideslope (solid black).

B. Example of Synchronized Relative Motion

An example of possible 3D forced relative motion occurring during close proximity operation is represented by the flyaround.

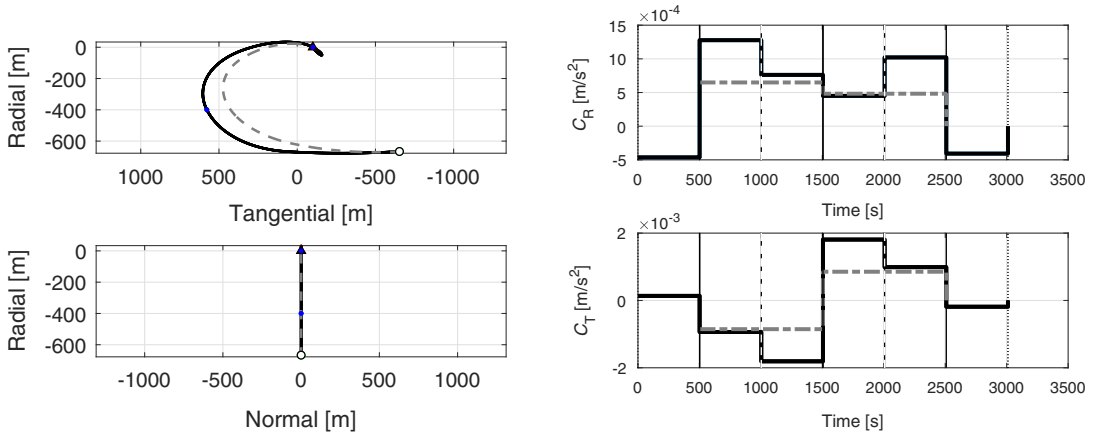

a) Trajectories $N = 2$. **b) Acceleration profiles $N = 2$.**

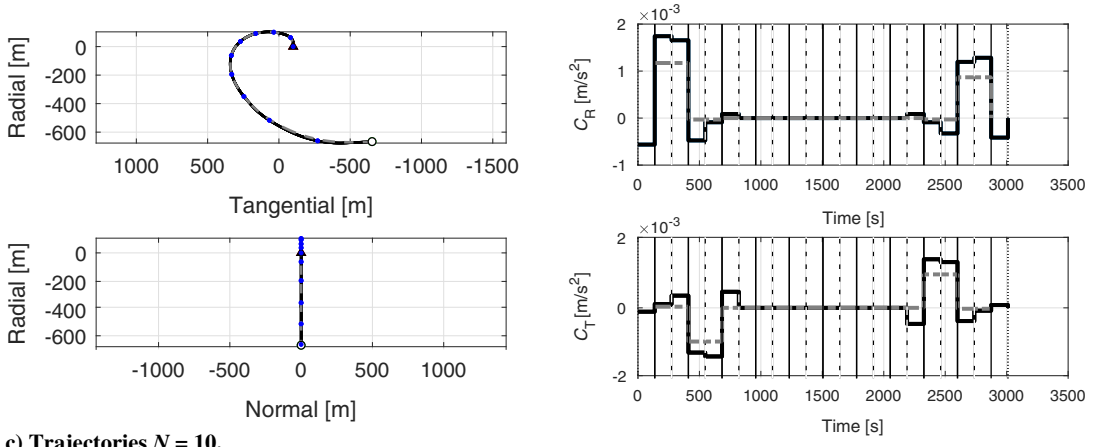

c) Trajectories $N = 10$. **d) Acceleration profiles $N = 10$.**

Fig. 7 In-plane reconfiguration: comparison between boundary (solid black) and centered (dashed gray) control grids, with different number of nodes.

This is typically required to synchronize a chaser spacecraft with the rotational motion of the target satellite, to inspect continuously a given point or to enable its robotic capture. When dealing with active debris removal activities, the target is generally non-cooperative (i.e., in real-time there is no exchange of information between the satellites) and noncollaborative (i.e., the target is not actively keeping an attitude that can aid during its capture). At the moment of the rendezvous, such targets have an unknown rotational dynamics and they are possibly tumbling. Even by adopting detumbling techniques devoted to damp the excessive rotational rate, a residual rotational motion is to be considered. Accordingly, a first step to understand the control action needed by a possible precapture phase is to assess required accelerations and corresponding delta-v budget for a forced circular relative trajectory in the plane perpendicular to the axis of rotation of the target. The impulsive guidance profile for such a motion can be designed following the flyaround method of [20], whereas the required continuous accelerations can be computed through the methodology presented in this Note.

As an example Fig. 8 reports the map of the equivalent delta-v costs for synchronized relative motion at a separation between the centers

Table 1 Summary of delta-v costs for the reconfiguration of Fig. 7

	Delta-v, m/s		
N maneuvers	Impulsive	Boundary grid	Centered grid
1	2.664	5.140	2.848
2	1.548	3.035	1.636
3	1.294	2.560	1.417
4	1.120	2.226	1.198
5	1.054	2.099	1.112

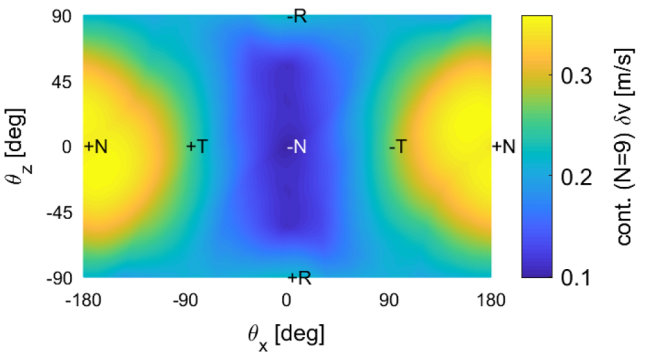

Fig. 8 Map of delta-v costs of all possible orientations of the rotational axis in RTN. Map obtained for $\omega = 0.1$ deg/s and $r_c = 10$ m.

of mass of the satellites r_c of 10 m and a residual angular rate of the target of 0.1 deg/s. The orientation of the axis of rotation into the RTN frame is expressed by adopting the θ_x and θ_z angles introduced in [20] to express its direction in the *local vertical/local horizontal orbital* frame. In particular, for this example the impulsive guidance is designed using $N = 9$ pulses. No final condition on the relative velocity after one loop is posed. As a consequence, when the chaser reaches again the initial relative position at time $N + 1$ (i.e., completes one loop) it has a velocity that will not make it to continue on the circumference for a second loop. For the sake of building a map, the initial conditions of each case are derived from the initial displacement of r_c while imposing null relative velocity at that point. Note that in general such relative state is not a stable condition for the relative dynamics, nor it might be the optimal starting point for the operational strategy of the capture. Nevertheless, this serves the

scope of providing comparable initial conditions for all the runs of the map, enabling a comparison between the different costs.

Following the considerations drawn in this Note, the centered grid is employed to derive the continuous acceleration profile and a minor adjustment is introduced to take into account the pulse at the starting time. The map of Fig. 8 provides the following results: the realistic delta-v budget associated with the different synchronization motions depending on the actual orientation of the rotational axis of the target satellite and the acceleration requirements for the propulsion system to enable that kind of motion. These results can be also used to support the operational tradeoff analysis between synchronization costs and possible redirection of the target spin axis by means of detumbling techniques. As expected from the equations of the relative dynamics, the cheapest flyaround is around the $-$N direction. By recalling the in-plane views of the natural relative orbits of Figs. 1 and 2, in fact, this condition requires only to circularize the relative in-plane trajectory without changing the verse of movement. On the contrary, a flyaround with respect to $+$N requires counteracting in full the relative effect of the gravitational pull. Note that the condition of a target satellite spinning around the normal direction is a very special situation, because it is fixed both in the inertial and in the local orbital frames. In general, for the robotic capture of non-cooperative targets, synchronization, precession of the rotational axis as seen in the local orbital frame, and straight-line approach have to be combined. Accordingly, the complete guidance plan has to be obtained combining the elementary solutions recalled in this Note. Once designed it, the methodology described here to retrieve the open-loop accelerations is applicable to the general case.

V. Conclusions

The equivalence between the linearized equations of the relative dynamics in Cartesian state and the linearized equations in relative orbital elements is proved through a Lyapunov transformation, for near-circular reference orbits. This is used to generate piecewise constant acceleration profiles from an available impulsive guidance solution: a sequence of two boundary problems are solved, each one covering intervals that contain two impulsive burns. The method is thought to support close-range proximity operations, which require larger maneuvers than formation keeping and reconfiguration, over limited time windows. For spaceborne autonomous applications it may be more convenient to solve the problem exploiting the impulsive approximation. However, it is shown that this introduces errors on the relative eccentricity and inclination vectors and on the relative mean argument of longitude if the error on the eccentricity vector is minimized. By comparing the trajectories obtained with impulsive and piecewise continuous controls, it is noted that they tend to overlap when the number of burns increases.

For the proposed approach it is important to properly set the structure of the control grid used to solve the two boundary problem. By analyzing the equations written in relative orbital elements, it is shown that a centered control grid minimizes the difference between the impulsive delta-v and the equivalent one from the piecewise continuous implementation. Moreover, by increasing the number of nodes the delta-v cost of the continuous implementation gets closer to the impulsive one.

Finally, the proposed method can be used to quickly assess delta-v cost and required accelerations to realize any given forced motion phase of close-proximity operations. As an example, the synchronized relative motion between a chaser spacecraft and a rotating target has been discussed.

Acknowledgments

The research leading to these results has received funding from the European Union's Horizon 2020 research and innovation program under the Marie Skłodowska-Curie grant agreement No. 793361–ReMoVE (Rendezvous Modelling Visiting and Enhancing).

References

[1] Liou, J.-C., "An Active Debris Removal Parametric Study for LEO Environment Remediation," *Advances in Space Research*, Vol. 47, No. 11, 2011, pp. 1865–1876. https://doi.org/10.1016/j.asr.2011.02.003

[2] Sullivan, J., Grimberg, S., and D'Amico, S., "Comprehensive Survey and Assessment of Spacecraft Relative Motion Dynamics Models," *Journal of Guidance, Control, and Dynamics*, Vol. 40, No. 8, 2017, pp. 1837–1859. https://doi.org/10.2514/1.G002309

[3] Gaias, G., Colombo, C., and Lara, M., "Analytical Framework for Precise Relative Motion in Low Earth Orbits," *Journal of Guidance, Control, and Dynamics*, Vol. 43, No. 5, 2020, pp. 915–927. https://doi.org/10.2514/1.G004716

[4] Gaias, G., D'Amico, S., and Ardaens, J.-S., "Generalized Multi-Impulsive Maneuvers for Optimum Spacecraft Rendezvous in Near-Circular Orbit," *International Journal of Space Science and Engineering*, Vol. 3, No. 1, 2015, pp. 68–88. https://doi.org/10.1504/IJSPACESE.2015.069361

[5] Montenbruck, O., Kirschner, M., D'Amico, S., and Bettadpur, S., "E/I-Vector Separation for Safe Switching of the GRACE Formation," *Aerospace Science and Technology*, Vol. 10, No. 7, 2006, pp. 628–635. https://doi.org/10.1016/j.ast.2006.04.001

[6] Gaias, G., and Ardaens, J.-S., "Design Challenges and Safety Concept for the AVANTI Experiment," *Acta Astronautica*, Vol. 123, June 2016, pp. 409–419. https://doi.org/10.1016/j.actaastro.2015.12.034

[7] D'Amico, S., and Montenbruck, O., "Proximity Operations of Formation Flying Spacecraft Using an Eccentricity/Inclination Vector Separation," *Journal of Guidance, Control and Dynamics*, Vol. 29, No. 3, 2006, pp. 554–563. https://doi.org/10.2514/1.15114

[8] Ardaens, J.-S., Gaias, G., and Kahle, R., "From GRACE to AVANTI: 15 Years of Formation-Flying Experience at DLR," *69th International Astronautical Congress*, International Astronautical Federation IAF, Paper IAC-18,D1,2,3, France, 2018.

[9] Clohessy, W. H., and Wiltshire, R. S., "Terminal Guidance System for Satellite Rendezvous," *Journal of the Aerospace Sciences*, Vol. 27, No. 9, 1960, pp. 653–658. https://doi.org/10.2514/8.8704

[10] Sinclair, A. J., Sherrill, R. E., and Lovell, T. A., "Calibration of Linearized Solutions for Satellite Relative Motion," *Journal of Guidance, Control, and Dynamics*, Vol. 37, No. 4, 2014, pp. 1362–1367. https://doi.org/10.2514/1.G000037

[11] D'Amico, S., "Relative Orbital Elements as Integration Constants of Hill's Equations," Deutsches Zentrum für Luft- und Raumfahrt TR DLR-GSOC TN 05-08, Oberpfaffenhofen, Germany, Dec. 2005.

[12] Gaias, G., Ardaens, J.-S., and Montenbruck, O., "Model of J2 Perturbed Satellite Relative Motion with Time-Varying Differential Drag," *Celestial Mechanics and Dynamical Astronomy*, Vol. 123, No. 4, 2015, pp. 411–433. https://doi.org/10.1007/s10569-015-9643-2

[13] D'Amico, S., "Autonomous Formation Flying in Low Earth Orbit," Ph.D. Thesis, Technical Univ. of Delft, Delft, The Netherlands, March 2010.

[14] Bennet, T., and Schaub, H., "Continuous-Time Modeling and Control Using Nonsingular Linearized Relative-Orbit Elements," *Journal of Guidance, Control, and Dynamics*, Vol. 39, No. 12, 2016, pp. 2605–2614. https://doi.org/10.2514/1.G000366

[15] Leonard, C. L., Hollister, W. M., and Bergmann, E. V., "Orbital Formationkeeping with Differential Drag," *Journal of Guidance, Control, and Dynamics*, Vol. 12, No. 1, 1989, pp. 108–113. https://doi.org/10.2514/3.20374

[16] Gaias, G., and D'Amico, S., "Impulsive Maneuvers for Formation Reconfiguration Using Relative Orbital Elements," *Journal of Guidance, Control, and Dynamics*, Vol. 38, No. 6, 2015, pp. 1036–1049. https://doi.org/10.2514/1.G000189

[17] Gaias, G., Ardaens, J.-S., and Colombo, C., "Precise Line-of-Sight Modelling for Angles-Only Relative Navigation," *Advances in Space Research*, Vol. 67, No. 11, 2021, pp. 3515–3526. https://doi.org/10.1016/j.asr.2020.05.048

[18] Larbi, M. B., and Stoll, E., "Spacecraft Formation Control Using Analytical Integration of Gauss' Variational Equations," *Proceedings of the 6th International Conference on Astrodynamics Tools and Techniques*, European Space Agency ESA, The Netherlands, 2016.

[19] Di Mauro, G., Bevilacqua, R., Spiller, D., Sullivan, J., and D'Amico, S., "Continuous Maneuvers for Spacecraft Formation Flying Reconfigura-

tion Using Relative Orbit Elements," *Acta Astronautica*, Vol. 153, Dec. 2018, pp. 311–326.
https://doi.org/10.1016/j.actaastro.2018.01.043

[20] Hablani, H. B., Tapper, M. L., and DanaBashian, D. J., "Guidance and Relative Navigation for Autonomous Rendezvous in a Circular Orbit," *Journal of Guidance, Control, and Dynamics*, Vol. 25, No. 3, 2002, pp. 553–562.
https://doi.org/10.2514/2.4916

[21] Ankersen, F., "Guidance, Navigation, Control and Relative Dynamics for Spacecraft Proximity Maneuvers," Ph.D. Thesis, Aalborg Univ., Aalborg, Denmark, Dec. 2010.

[22] Gaias, G., and Lovera, M., "Safe Trajectory Design for Close Proximity Operations," *2020 AAS/AIAA Astrodynamics Specialist Conference*, American Astronautical Soc. Paper 20-641, Univelt, Inc., San Diego, CA, 2020.